Postinflationary production of particle dark matter: Hilltop and Coleman-Weinberg inflation

Anish Ghoshal[,1,*] Maxim Yu. Khlopov,[2,3,4,†] Zygmunt Lalak,[1,‡] and Shiladitya Porey[5,§]

[1]*Institute of Theoretical Physics, Faculty of Physics, University of Warsaw,*
Ludwika Pasteura 5, 02-093 Warsaw, Poland
[2]*Virtual Institute of Astroparticle physics, 75018 Paris, France*
[3]*Institute of Physics, Southern Federal University, 344090 Rostov on Don, Russia*
[4]*National Research Nuclear University "MEPHI", 115409 Moscow, Russia*
[5]*Department of Physics, Novosibirsk State University, Pirogova 2, 630090 Novosibirsk, Russia*

We investigate the production of nonthermal dark matter (DM), χ, during the postinflationary reheating era. For inflation, we consider two slow roll single field inflationary scenarios—generalized version of Hilltop (GH) inflation, and Coleman-Weinberg (CW) inflation. Using a set of benchmark values that comply with the current constraints from cosmic microwave background radiation (CMBR) data for each inflationary model, we explored the parameter space involving mass of dark matter particles, m_χ, and coupling between inflaton and χ, y_χ. For these benchmarks, we find that tensor-to-scalar ratio r can be as small as 2.69×10^{-6} for GH and 1.91×10^{-3} for CW inflation, both well inside 1-σ contour on scalar spectral index versus r plane from *Planck*2018+BICEP3+*Keck Array*2018 dataset, and testable by future cosmic microwave background (CMB) observations, e.g., Simons Observatory. For the production of χ from the inflaton decay satisfying CMB and other cosmological bounds and successfully explaining total cold dark matter density of the present universe, we find that y_χ should be within this range $\mathcal{O}(10^{-4}) \gtrsim y_\chi \gtrsim \mathcal{O}(10^{-20})$ for both inflationary scenarios. We also show that, even for the same inflationary scenario, the allowed parameter space on reheating temperature versus m_χ plane alters with inflationary parameters including scalar spectral index, r, and energy scale of inflation.

I. INTRODUCTION

The ΛCDM (Λcold dark matter) cosmological model of the universe is undoubtedly successful in explaining not only the origin of the universe and its transformation from a very hot to a cold stage but also accurately depicts each cosmological epoch from the era of big bang nucleosynthesis up to the present-day universe. After the observation and subsequent analysis of cosmic microwave background data obtained from COBE, *WMAP*, and later from the *Planck* mission, this cosmological model was bolstered. However, the ΛCDM model, along with the standard model of particle physics, fails to shed light on the nature of DM.

*anish.ghoshal@fuw.edu.pl
†khlopov@apc.in2p3.fr
‡zygmunt.lalak@fuw.edu.pl
§shiladityamailbox@gmail.com

There is a possibility that DM can potentially exist in the form of primordial black holes (PBHs) or massive compact halo objects (MACHOs), but it cannot account for the total density of cold dark matter (CDM) [1,2]. Therefore, DM is believed to be in the form of particles, specifically beyond the standard model (BSM) particles, such as the popular candidate known as weakly interacting massive particles (WIMPs). These particles were expected to be in thermal equilibrium with the standard model particles, also known as radiation, in the early hot universe and subsequently decoupled at a later stage, depending on the temperature of radiation, the mass of the WIMP, and the cross section of its interaction with standard model particles. However, the failure of particle detectors to detect the presence of WIMPs has led to the consideration of alternative scenarios, such as feebly interacting massive particles (FIMPs), which were never in thermal equilibrium with radiation [3–11]. Consequently, the number density of FIMP is independent of initial number density and can be produced either from decay of massive particles, such as moduli field or curvaton [12] or inflaton, or from the scattering of standard model (SM) particle or inflaton via gravitational interaction [13–17]. If these feebly interacting particles are

not massive, they can also contribute to other observables like the measurements of dark radiation as ΔN_{eff} in CMB etc. [18,19].

In addition to supporting ΛCDM, precise measurements of the cosmic microwave background (CMB) also reveal that the proper explanation for some features of the universe ΛCDM model fails to incorporate. These problems include large-scale homogeneity, nearly small values of inhomogeneity, and description of the formation of large-scale structures. In this context, a short period of exponential expansion known as cosmic inflation [20–23] during the infant universe has the ability to address these issues. In general, dark matter and inflation are unrelated scenarios. Nonetheless, inflation and reheating both form the frameworks for the production of particles beyond the SM of particles. Since we know the SM cannot accommodate DM particle, and it must be from beyond the SM sector, it is naturally very interesting to look for the possibility of the production of dark matter particles during inflation. Following the inflationary era, a period of reheating is also required to make the universe hot and dominated by relativistic standard model particles, commonly referred to as radiation. The simplest possibility is that the universe is driven by a single scalar field, the inflaton, which is a Standard Model gauge singlet studied in several works [24,25]. After the BICEP + PLANCK observations, inflationary potentials with concave shapes or flat potentials for the inflaton have gained favorability. Models incorporating nonminimal couplings between inflaton and Ricci scalar have been extensively explored (e.g. Refs. [26–37]). Additionally, there are several models that consider flat potentials without coupling, such as inflection point inflation. These models can also incorporate dark matter, such as SMART $U(1)_X$ [38] (see also [39–41]), model with a single axionlike particle [42], the νMSM [43], the NMSM [44], the WIMPflation [45], and extension with a complex flavon field [46]. Very recently testability of FIMP DM involving long-lived particle searches at laboratories involving various portals (categorized via spin of the mediators) [47–53] and involving primordial gravitational waves of inflationary origin have been proposed [18,54–56].

In this work, alongside our previous work [57], we address both the inflation and dark matter including two different BSM fields, one is boson and another one is fermion. For the inflationary part we have considered Hilltop inflation. Any inflationary potential can be approximated as Hilltop near its maximum. Then we have considered Coleman-Weinberg inflation. We derive the conditions on DM parameter space from the analysis of inflationary constraint and constraints on inflaton-DM couplings, inflaton and DM masses based on DM phenomenology.

The paper is organized as follows: we begin in Sec. II where we introduce the Lagrangian density of our model. In Sec. III, we study the slow-roll inflationary scenario,

reheating, and production of DM in generalized Hilltop scenario with canonical kinetic energy of the inflaton. Following this, in Sec. IV, we explore the same aspects for Coleman-Weinberg inflation. Finally, we summarize our results in Sec. V.

In this work, we assume that the spacetime metric is diagonal with signature $(+, -, -, -)$. We also use $\hbar = c = k_B = 1$ unit in which reduced Planck mass is $M_P = 2.4 \times 10^{18}$ GeV.

II. LAGRANGIAN DENSITY

In addition to the Standard Model (SM) Higgs field H our model includes two other beyond the standard model (BSM) fields: a real scalar inflaton ϕ and a vectorlike singlet (under SM gauge groups) fermionic field χ that plays the role of a nonthermal DM. As a result, we write the action as [58–62]

$$\mathcal{S} = \int \mathrm{d}x^4 \sqrt{-g}(\mathcal{L}_{\text{INF}}(\mathcal{R}, \phi) + \mathcal{L}_{\chi} + \mathcal{L}_H + \mathcal{L}_{\text{rh}}). \quad (1)$$

Here, g and $\mathcal{R}$ are the determinant of spacetime metric and curvature scalar, respectively, and $\mathcal{L}_{\text{INF}}(\mathcal{R}, \phi)$ is the Lagrangian density of the slow-roll inflationary scenario driven by ϕ, and the Lagrangian density of χ and SM Higgs doublet H are as follows:

$$\mathcal{L}_{\chi} = i\bar{\chi}\partial\!\!\!/\chi - m_{\chi}\bar{\chi}\chi, \quad (2)$$

$$\mathcal{L}_H = (\partial H)^2 + m_H^2 H^{\dagger}H - \lambda_H (H^{\dagger}H)^2, \quad (3)$$

where $\partial\!\!\!/$ is the Dirac operator in Feynman's slash notation, m_{χ} and m_H both have the mass dimension whereas λ_H is dimensionless. Since we consider production of DM particle, χ, and SM Higgs particle, h, during reheating era, we can write the interaction Lagrangian as

$$\mathcal{L}_{\text{rh}} = -y_{\chi}\phi\bar{\chi}\chi - \lambda_{12}\phi H^{\dagger}H - \lambda_{22}\phi^2 H^{\dagger}H + \mathcal{L}_{\text{scatter}} + \text{H.c.} \quad (4)$$

where $\mathcal{L}_{\text{scatter}}$ includes higher order terms that account for the scattering of χ by inflaton, or SM particles (including H). The couplings y_{χ} and λ_{22} are also dimensionless but λ_{12} has mass dimension. Now, in the following sections, we analyze two inflationary models while considering benchmark values that satisfy current constraints from CMB. Additionally, with the assumption that the DM is produced during reheating era, we explore the parameter space involving y_{χ} and m_{χ} such that χ becomes accountable for the total CDM density of the present universe.

III. GENERALIZED HILLTOP

One of the papers [63] from *Planck* 2018 collaboration features a set of single field slow-roll inflationary scenarios,

TABLE I. Benchmark values for GH inflation ($\mathcal{N}_{\mathrm{CMB}} \approx 60$).

Benchmark		ϕ_0/M_P	ϕ_*/M_P	ϕ_{end}/M_P	V_0	n_s	r
GH-BM1	$m = 10, n = 2$	16	10.0544	14.9705	9.4255×10^{-11}	0.96473	2.9754×10^{-3}
GH-BM2	$m = 15, n = 2$	1	0.4606	0.6284	8.3643×10^{-14}	0.964736	2.6918×10^{-6}
GH-BM3	$m = 4, n = 2$	20	9.7845	18.7226	6.9045×10^{-10}	0.964597	1.9747×10^{-2}

with Hilltop inflation being one of them. This specific model with potential of the form $\Lambda^4(1 - \phi^4/\mu_4^4 + \cdots)$ and with $-2 < \log_{10}(\mu_4/M_P) < 2$ satisfies predictions within 1-σ C.L. on (n_s, r) plane. The three dots represent the missing higher order terms, which are expected to stabilize the potential from below just after the end of inflation and prevent the universe from collapsing. Although, for $\phi_0 \ll M_P$, terms of higher order of (ϕ/ϕ_0) can be added to the potential to stabilize without altering the (n_s, r) predictions, the predicted value of n_s of this inflationary model is small compared to the current best fit value obtained from *Planck* 2018 [64–66]. However, the most recent combined data of *B*-mode of polarization of CMB from *Planck*, *WMAP*, and BICEP/*Keck* strongly favors a concave rather than convex shape of the inflationary potential. Any concave potential can be approximated as a Hilltop potential around the local maximum [67]. Thus, in this work, we consider a generalized form of the Hilltop potential and thus this inflationary model is referred as generalized Hilltop (abbreviated as GH) inflationary scenario. The Lagrangian density and potential density of this inflationary model are given by [67,68] (see also [64–66,69–71])

$$\mathcal{L}_{\mathrm{INF}}(\mathcal{R}, \phi) = \frac{M_P^2}{2} \mathcal{R} + \frac{1}{2} \partial_\mu \phi \partial^\nu \phi - V_{\mathrm{GH}}(\phi), \quad (5)$$

$$V_{\mathrm{GH}}(\phi) = V_0 \left(1 - \left(\frac{\phi}{\phi_0} \right)^m \right)^n, \quad (6)$$

where V_0 and ϕ_0 have the mass dimension of 4 and 1, respectively. We expect both V_0 and ϕ_0 are positive. In Eq. (6), if either of m, n, or both are fractions, the potential has discontinuity either at $\phi = 0$ or at $\phi = \phi_0$. However, if both m, and n are positive integers, the potential is continuous at both $\phi = 0$ and $\phi = \phi_0$. Henceforth, we consider only positive integer values of m and n. Moreover, when n is positive integer (and for $\phi_0 > 0$), the inflaton descends along the slope of the $V_{\mathrm{GH}}(\phi)$ from small to large values of ϕ. Additionally, for positive integer value of n, the potential is symmetric (asymmetric) about the origin if m is an even (odd) number. If n is an even number (with a positive integer value of m), then the potential is bounded from below. The potential in Eq. (6) can have two stationary points: $V'_{\mathrm{GH}}(\phi) = 0$ at $\phi = 0$ if $m > 1$, $V'_{\mathrm{GH}}(\phi) = 0$ at $\phi = \phi_0$ if $n > 1$. Here (and also throughout

this article), prime denotes derivative with respect to ϕ. Additionally, $V''_{\mathrm{GH}}(\phi) = 0$ at $\phi = 0$ for $m > 2$ and $V''_{\mathrm{GH}}(\phi) = 0$ at $\phi = \phi_0$ for $n > 2$. Therefore, we choose $n = 2$ such that $V_{\mathrm{GH}}(\phi)$ remains continuous, finite, real, and bounded from below for $\phi \geq \phi_0$ and also there exists a minimum at $\phi = \phi_0$. When $n = m = 2$, (n_s, r) prediction for that potential does not match well with the CMB data [67]. Thus, we choose $m > n$ which is also needed to satisfy n_s from the current CMB bound, as shown in Ref. [67]. The chosen benchmark values for GH inflation are shown in Table I. Benchmark GH-BM1 is for large field inflation, while GH-BM2 is for small field inflation. Benchmark GH-BM3 is for the inflationary scenario described in Ref. [68].

The slow-rolling condition of the inflation is generally expressed in terms of potential-slow-roll parameters. The first two potential-slow-roll parameters for a single inflaton whose kinetic energy is minimally connected to gravity, as in Eq. (5), are defined as

$$\epsilon_V(\phi) = \frac{M_P^2}{2} \left(\frac{V'_{\mathrm{GH}}(\phi)}{V_{\mathrm{GH}}(\phi)} \right)^2 = M_P^2 \frac{m^2 n^2 \phi^{2m-2}}{2(\phi^m - \phi_0^m)^2}, \quad (7)$$

$$\eta_V(\phi) = M_P^2 \frac{V''_{\mathrm{GH}}(\phi)}{V_{\mathrm{GH}}(\phi)}$$
$$= M_P^2 \frac{mn\phi^{m-2}((mn-1)\phi^m - (m-1)\phi_0^m)}{(\phi^m - \phi_0^m)^2}. \quad (8)$$

In order to maintain slow roll inflation, it is required that both ϵ_V, and $|\eta_V|$ are < 1. If either condition is violated, it signals the end of the slow roll inflationary epoch. The duration of inflation is parameterized in terms of the number of e-folds, $\mathcal{N}_{\mathrm{CMB}}$, which indicates the amount of exponential expansion of the cosmological scale factor a or the amount of reduction of comoving Hubble radius $[(a\mathcal{H})^{-1}, \mathcal{H}$ being the Hubble parameter] that occurs during inflation, is defined as

$$\mathcal{N}_{\mathrm{CMB}} = \frac{1}{M_P^2} \int_{\phi_{\mathrm{end}}}^{\phi_*} \frac{V_{\mathrm{GH}}(\phi)}{V'_{\mathrm{GH}}(\phi)} \, d\phi. \quad (9)$$

Here, ϕ_{end} is the value of the inflaton when inflation ends, and ϕ_* is the value of inflaton at which the cosmic length-scale of CMB observation corresponding to e-fold $\mathcal{N}_{\mathrm{CMB}}$ leaves the comoving Hubble radius during inflation.

TABLE II.   Constraints on inflationary parameters from CMB experiments.

$\ln(10^{10}A_s)$	3.044 ± 0.014	68%, TT, TE, EE + lowE + lensing + BAO	[76,77]
n_s	0.9647 ± 0.0043	68%, TT, TE, EE + lowE + lensing + BAO	[76]
r	$0.014^{+0.010}_{-0.011}$ and	95%, BK18, BICEP3, *Keck Array* 2020,	[76,78,79]
	< 0.036	and *WMAP* and *Planck* CMB polarization	(see also [80])

$\mathcal{N}_{\rm CMB} \geq 60$ is required to solve Horizon problem [72]. Therefore, in this work, we choose benchmark values corresponding to $\mathcal{N}_{\rm CMB} \approx 60$.

Cosmic inflation, on the other hand, conjures scalar and tensor perturbations. The kth Fourier mode of the quantum fluctuations departs the Hubble horizon when it becomes $k < \mathcal{H}$. This happens because the radius of comoving Hubble horizon shrinks during inflation. Following that, kth mode becomes super horizon and frozen. When the inflation ends and the comoving Horizon begins to expand again during radiation or matter domination, this kth mode may reenter the causal area. After reentering, the statistical nature of the kth Fourier mode of scalar (or density perturbation) and tensor perturbation can be expressed in terms of the power spectrum (parametrized in power law form) as

$$\mathcal{P}_s(k) = A_s\left(\frac{k}{k_*}\right)^{n_s - 1 + (1/2)\alpha_s \ln(k/k_*) + (1/6)\beta_s (\ln(k/k_*))^2}, \quad (10)$$

$$\mathcal{P}_h(k) = A_t\left(\frac{k}{k_*}\right)^{n_t + (1/2)dn_t/d\ln k \ln(k/k_*) + \cdots}, \quad (11)$$

where A_s, A_t, n_s, n_t, α_s, and β_s are respectively amplitude of scalar and tensor primordial power spectrum, scalar and tensor spectral index, running of scalar spectrum index, and running of running of scalar spectral index. Moreover, k_* is the pivot scale at which A_s is independent of n_s. Additionally, at this scale, constraints on the inflationary observables are drawn from CMB measurements. k_* also corresponds to ϕ_* around which the inflationary potential is constructed. Now, n_s can be estimated using potential-slow-roll parameters at leading order as

$$n_s = 1 - 6\epsilon_V(\phi_*) + 2\eta_V(\phi_*). \quad (12)$$

On the other hand, the definition of tensor-to-scalar ratio under the assumption of slow roll approximation, is

$$r = \frac{A_t}{A_s} \approx 16\epsilon_V(\phi_*). \quad (13)$$

Using Eq. (13), we can define A_s for $V_{\rm GH}(\phi)$ as

$$A_s \approx \frac{V_{\rm GH}(\phi_*)}{24\pi^2 M_P^4 \epsilon_V} \approx \frac{2V_{\rm GH}(\phi_*)}{3\pi^2 M_P^4 r}. \quad (14)$$

The latest bound on A_s, n_s, and r are listed in Table II, where T and E stand for the temperature and E-mode polarization of CMB. We choose the benchmark values of the inflationary scenario of Eqs. (5) and (6) in Table I such that the conditions from Table II are satisfied, and Fig. 1 displays the (n_s, r) predictions for those benchmark values along with the 1-σ (98% C.L.) and 2-σ (65% C.L.) contour (current bound and prospective future reach) on $n_s - r$ plane from current and future CMB observations. The predicted value of $(n_s \cdot r)$ of both GH-BM1 and GH-BM3 are within 1-σ contour of *Planck*2018+BICEP3 (2022) +*Keck Array*2018. Furthermore, the predicted value of $(n_s \cdot r)$ of GH-BM1 falls even within the region of prospective future reach of SO at 2-σ best-fit contour. Figure 1 also shows that the estimated value of r for benchmark GH-BM2 is very small, which is expected as it is derived for small field inflationary scenario. Due to the small value of r, this benchmark can only be tested by future CMB experiments, e.g., CMB-S4.
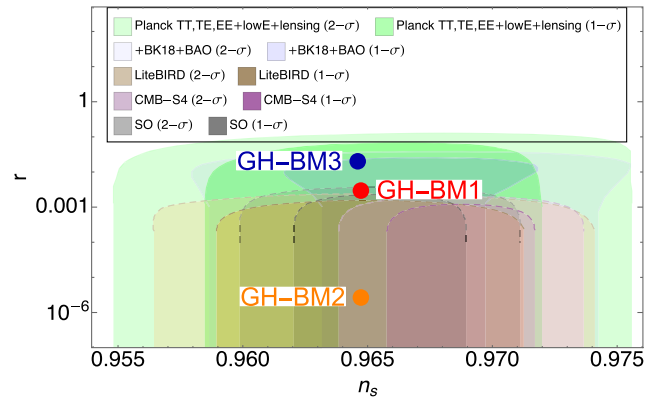

FIG. 1.   The predicted values of n_s, r for the three benchmark values from Table I are displayed as colored circular dots. The $n_s - r$ contours at 1-σ and 2-σ C.L. from present and future CMB observations are also displayed in the background. We use the deep colored region (located inside) for 95% (1-σ C.L.) and the light colored region (located outside) for 68% (2-σ C.L.) best-fit contours. The bound on (n_s, r) plane from the *Planck* 2018 is indicated by the green colored region, while bound from combined *Planck* 2018+BICEP3 (2022)+*Keck Array*2018 is indicated by the blue-shaded region. Other colored regions, with dashed lines as their boundary, indicate contours from future CMB experiments with higher sensitivity—such as *LiteBIRD*, CMB-S4, and Simons Observatory (SO) [73–75].

TABLE III. Allowed upper limit of y_χ and λ_{12} for the benchmark values from Table I.

Benchmark	Stability for y_χ		Stability for λ_{12}	
	About $\mu = \phi_*$	About $\mu = \phi_{\mathrm{end}}$	About $\mu = \phi_*$	About $\mu = \phi_{\mathrm{end}}$
GH-BM1	$y_\chi < 2.5051 \times 10^{-4}$	$y_\chi < 3.8572 \times 10^{-4}$	$\lambda_{12}/M_P < 1.2757 \times 10^{-6}$	$\lambda_{12}/M_P < 2.1619 \times 10^{-6}$
GH-BM2	$y_\chi < 2.7183 \times 10^{-4}$	$y_\chi < 6.5637 \times 10^{-4}$	$\lambda_{12}/M_P < 1.2413 \times 10^{-7}$	$\lambda_{12}/M_P < 9.9151 \times 10^{-7}$
GH-BM3	$y_\chi < 5.3167 \times 10^{-4}$	$y_\chi < 3.7039 \times 10^{-4}$	$\lambda_{12}/M_P < 5.3244 \times 10^{-6}$	$\lambda_{12}/M_P < 1.1649 \times 10^{-6}$

A. Stability analysis

In this subsection, we estimate the maximum permissible value of y_χ and λ_{12}[1] [defined in Eq. (4)] such that the flatness of the inflationary potential does not get destabilized from the radiative correction emerging from interaction of inflaton with other fields, e.g., χ and H. For this, we need to consider Coleman–Weinberg radiative correction at 1-loop order to the inflaton-potential which is [82]

$$V_{\text{1-loop}} = \sum_j \frac{n_j}{64\pi^2} (-1)^{2s_j} \tilde{m}_j^4 \left[\ln\left(\frac{\tilde{m}_j^2}{\mu^2}\right) - c_j \right]. \quad (15)$$

Here, $j \equiv H, \chi, \phi$, and $c_j = \frac{3}{2}$; $n_{H,\chi} = 4$, $n_\phi = 1$; $s_H = 0$, $s_\chi = 1/2$, and $s_\phi = 0$. In this work, we assume two values of the renormalization scale: $\mu = \phi_*$ and $\mu = \phi_{\mathrm{end}}$. Meanwhile, the inflaton dependent mass of H and χ are

$$\tilde{m}_\chi^2(\phi) = (m_\chi + y_\chi \phi)^2, \qquad \tilde{m}_H^2(\phi) = m_H^2 + \lambda_{12}\phi. \quad (16)$$

Now, the first and second derivatives of the Coleman-Weinberg term for χ and H with respect to ϕ are

$$V'_{\text{1-loop}} = \sum_j \frac{n_j}{32\pi^2} (-1)^{2s_j} \tilde{m}_j^2 (\tilde{m}_j^2)' \left[\ln\left(\frac{\tilde{m}_j^2}{\mu^2}\right) - 1 \right], \quad (17)$$

$$V''_{\text{1-loop}} = \sum_j \frac{n_j}{32\pi^2} (-1)^{2s_j} \left\{ \left[\left((\tilde{m}_j^2)' \right)^2 + \tilde{m}_j^2 (\tilde{m}_j^2)'' \right] \right.$$
$$\left. \times \ln\left(\frac{\tilde{m}_j^2}{\mu^2}\right) - \tilde{m}_j^2 (\tilde{m}_j^2)'' \right\}. \quad (18)$$

Using Eq. (16) in Eqs. (17) and (18), we get Coleman-Weinberg correction term for H and χ as (with $m_\chi = m_H = 0$)

$$|V'_{\text{1-loop},H}| = \frac{\lambda_{12}^2 \phi}{8\pi^2} \left(\ln\left(\frac{\lambda_{12}\phi}{\mu^2}\right) - 1 \right),$$

$$|V'_{\text{1-loop},\chi}| = \frac{\Phi^3 y_\chi^4}{4\pi^2} \left(1 - \ln\left(\frac{\phi^2 y_\chi^2}{\mu^2}\right) \right), \quad (19)$$

$$|V''_{\text{1-loop},H}| = \frac{\lambda_{12}^2}{8\pi^2} \ln\left(\frac{\lambda_{12}\phi}{\mu^2}\right).$$

$$|V''_{\text{1-loop},\chi}| = \frac{1}{8\pi^2} \left(6\phi^2 y_\chi^4 \ln\left(\frac{\phi^2 y_\chi^2}{\mu^2}\right) - 2\phi^2 y_\chi^4 \right). \quad (20)$$

Let us define tree level potential $V_{\text{tree}}(\phi)$ as $V_{\text{tree}}(\phi) \equiv V_{\mathrm{GH}}(\phi)$. Then

$$V'_{\text{tree}}(\phi) \equiv V'_{\mathrm{GH}}(\phi) = -mn \frac{V_0}{\phi} \left(\frac{\phi}{\phi_0}\right)^m \left(1 - \left(\frac{\phi}{\phi_0}\right)^m\right)^{n-1} \quad (21)$$

$$V''_{\text{tree}}(\phi) \equiv V''_{\mathrm{GH}}(\phi) = mn \frac{V_0}{\phi^2} \left(\frac{\phi}{\phi_0}\right)^m \left(1 - \left(\frac{\phi}{\phi_0}\right)^m\right)^{n-2}$$
$$\times \left((mn - 1)\left(\frac{\phi}{\phi_0}\right)^m - m + 1 \right), \quad (22)$$

Maintaining the stability of the inflation-potential, the maximum allowed value of λ_{12} and y_χ can be obtained when all the following conditions are satisfied at $\phi = \mu$

$$|V'_{\text{1-loop},H}(\phi = \mu)| < V'_{\text{tree}}(\phi = \mu),$$
$$|V'_{\text{1-loop},\chi}(\phi = \mu)| < V'_{\text{tree}}(\phi = \mu), \quad (23)$$

$$|V''_{\text{1-loop},H}(\phi = \mu)| < V''_{\text{tree}}(\phi = \mu),$$
$$|V''_{\text{1-loop},\chi}(\phi = \mu)| < V''_{\text{tree}}(\phi = \mu). \quad (24)$$

The permitted upper limit for the couplings y_χ and λ_{12} for GH inflationary scenario are listed in Table III for $\mu = \phi_*$ and $\mu = \phi_{\mathrm{end}}$. From this table, we conclude that the permissible upper limit of the couplings are: $y_\chi < 2.5051 \times 10^{-4}, < 2.7183 \times 10^{-4}, < 3.7039 \times 10^{-4}$, and $\lambda_{12}/M_P < 1.2757 \times 10^{-6}, < 1.2413 \times 10^{-7}, < 1.1649 \times 10^{-6}$ for GH-BM1, GH-BM2, and GH-BM3, respectively.

---

[1]While the quadratic coupling λ_{22} does play a role during reheating, the stability analysis presented in this section indicates a very small permissible upper value for λ_{22} [81]. Therefore, our primary focus in this article has been on the coupling λ_{12} since we are interested in perturbative approach of reheating.

B. Reheating era and production of DM

As soon as the slow-roll inflationary phase terminates, inflaton quickly descends to the minimum of the potential and starts coherent oscillations about the minimum of the potential. The minimum of the potential of Eq. (6) is ϕ_0 (for the chosen benchmark values of Table I) and thus, the physical mass of the inflaton is [83]:

$$\frac{m_\phi}{M_P} = (M_P^{-2} V''_{\mathrm{GH}}(\phi)|_{\phi=\phi_0})^{1/2}. \tag{25}$$

If we define two dimensionless variables $\mathbb{x} = \phi/M_P$ and $\mathbb{x}_0/M_P$, then, we are assuming that expanding the potential $V_{\mathrm{GH}}(\mathbb{x})$ about the minimum, $\mathbb{x}_0$, we get (for $(\phi - \phi_0) \ll 1 \Rightarrow (\mathbb{x} - \mathbb{x}_0) \ll 1$)

$$V_{\mathrm{GH}}(\mathbb{x} - \mathbb{x}_0) = -mV_0 \frac{(\mathbb{x} - \mathbb{x}_0)^n}{\mathbb{x}_0} + \quad \text{(smaller terms).} \tag{26}$$

Since we choose $n = 2$ for three benchmark values,[2] the energy density of inflaton and pressure, averaging over an oscillating cycle during reheating, behaves as [83] (see also [84])

$$\rho_\phi \propto a^{-3}, \qquad \langle p \rangle = 0. \tag{27}$$

This oscillating inflaton begins to produce χ and relativistic Higgs particles h following Eq. (4) and initiates the reheating era. This is a highly adiabatic epoch during which the universe changes from being cold and dominated by the energy density of oscillating inflaton to hot visible universe. The relativistic SM particles produced during reheating era eventually thermalize among themselves and develop the local-thermal fluid of the universe. As a result of that the energy density of radiation, ρ_{rad}, and temperature of the universe, T, both increase, while ρ_ϕ decreases. However, χ being feebly interacting with the SM particles, it may not share the same temperature as that of SM plasma. Sooner, the energy density of oscillating inflaton becomes equal to that of relativistic SM particles. The temperature of the universe at that particular moment is referred to as the reheating temperature, denoted by T_{rh}, which can be estimated as [58]:

$$T_{\mathrm{rh}} = \sqrt{\frac{2}{\pi}} \left(\frac{10}{g_\star}\right)^{1/4} \sqrt{M_P} \sqrt{\Gamma_\phi}, \tag{28}$$

where $g_\star = 106.75$ is effective number of degrees of freedom of relativistic fluid of the universe and Γ_ϕ is the total decay width of inflaton. At the beginning of reheating

---

[2]For example, we assume $\frac{17}{4} \frac{(\mathbb{x} - \mathbb{x}_0)^2}{dz_0^2} \ll 3 \frac{(\mathbb{x} - \mathbb{x}_0)}{\mathbb{x}_0} \ll 1$ for GH-BM3.

era, on the other hand, $\mathcal{H}$ is greater than Γ_ϕ. Then, $\mathcal{H}$ continues to decrease and it becomes $\mathcal{H}(T_{\mathrm{rh}}) \sim \Gamma_\phi$, where $\mathcal{H}(T_{\mathrm{rh}})$ is the value of Hubble parameter when the temperature of the universe is T_{rh}. After this, ρ_ϕ is transferred completely and almost immediately to ρ_{rad} and the universe becomes radiation dominated.

It is expected that at the beginning of the reheating epoch, ρ_ϕ decreases relatively at a faster rate, leading a quick rise of the temperature of the universe. However, after some initial increase of temperature, the Hubble expansion comes into play, causing the temperature to decrease. The maximum attainable temperature during reheating process can be estimated as [85,86]:

$$T_{\max} = \Gamma_\phi^{1/4} \left(\frac{60}{g_\star \pi^2}\right)^{1/4} \left(\frac{3}{8}\right)^{2/5} \mathcal{H}_I^{1/4} M_P^{1/2}, \tag{29}$$

where $\mathcal{H}_I$ is the value of Hubble parameter at the beginning of reheating era when $\rho_{\mathrm{rad}} = 0$ [85], i.e.,

$$\mathcal{H}_I = \sqrt{\frac{V_{\mathrm{GH}}(\phi_{\mathrm{end}})}{3M_P^2}}, \tag{30}$$

i.e., we assume in this work that $\mathcal{H}_I$ is the value Hubble parameter when slow roll inflation ends. $T_{\max} > T_{\mathrm{rh}}$ indicates that a particle of mass $> T_{\mathrm{rh}}$ can still be produced during reheating. Furthermore, in many cases, the amount of DM produced during reheating depends on the ratio $T_{\max}/T_{\mathrm{rh}}$ (for example, see Refs. [87,88]). Then, from Eqs. (28) and (29) we get:

$$\frac{T_{\max}}{T_{\mathrm{rh}}} = \left(\frac{3}{8}\right)^{2/5} \left(\frac{\mathcal{H}_I}{\mathcal{H}(T_{\mathrm{rh}})}\right)^{1/4}, \tag{31}$$

where we have used $\mathcal{H}(T_{\mathrm{rh}}) = (2/3)\Gamma_\phi$ [58]. At $T = T_{\mathrm{rh}}$, the universe is radiation dominated and thus

$$\mathcal{H}^2(T_{\mathrm{rh}}) = \frac{1}{3M_P^2} \left(\frac{\pi^2}{30} g_\star T_{\mathrm{rh}}^4\right). \tag{32}$$

Since, we are not considering any variation of $g_\star$ during reheating era, $(T_{\max}/T_{\mathrm{rh}}) \propto \mathcal{H}_I^{1/4} T_{\mathrm{rh}}^{-1/2}$. As a result, for a specific benchmark, $\mathcal{H}_I$ is fixed and, therefore, $(T_{\max}/T_{\mathrm{rh}})$ decreases as T_{rh} increases. In this work, we confine our discussion to perturbative approach of reheating [89]. The decay width of inflaton to χ and h and total decay width of inflaton are [58] (here we neglect the effect of thermal mass [90])

$$\Gamma_{\phi \to hh} \simeq \frac{\lambda_{12}^2}{8\pi m_\phi}, \qquad \Gamma_{\phi \to \chi\chi} \simeq \frac{y_\chi^2 m_\phi}{8\pi},$$

$$\Gamma_\phi = \Gamma_{\phi \to hh} + \Gamma_{\phi \to \chi\chi} \approx \Gamma_{\phi \to hh}. \tag{33}$$

TABLE IV. $m_\phi, \Gamma_\phi, T_{\rm rh}$, and $\mathcal{H}_I$ for the benchmark values from Table I.

Benchmark	m_ϕ/M_P (Sec. III B)	$\Gamma_\phi M_P$ [Eq. (33)]	$T_{\rm rh}/\lambda_{12}$ [Eq. (28)]	$\mathcal{H}_I/M_P$ [Eq. (30)]
GH-BM1	8.5812×10^{-6}	$4636.73\lambda_{12}^2$	30.0576	2.7228×10^{-6}
GH-BM2	6.1351×10^{-6}	$6485.42\lambda_{12}^2$	35.5482	1.6682×10^{-7}
GH-BM3	7.4321×10^{-6}	$5353.64\lambda_{12}^2$	32.2978	3.5200×10^{-6}

The assumption $\Gamma_\phi \sim \Gamma_{\phi \to hh}$ is necessary to avoid of DM domination from occurring just after the reheating era. The branching fraction for the production of χ from the decay-channel then can be defined as

$$\text{Br} = \frac{\Gamma_{\phi \to \chi\chi}}{\Gamma_{\phi \to \chi\chi} + \Gamma_{\phi \to hh}} \simeq \frac{\Gamma_{\phi \to \chi\chi}}{\Gamma_{\phi \to hh}} = m_\phi^2 \left(\frac{y_\chi}{\lambda_{12}}\right)^2. \quad (34)$$

Now, Table IV presents the values of $m_\phi, \Gamma_\phi, T_{\rm rh}$, and $\mathcal{H}_I$ for the benchmark values mentioned in Table I. Out of three benchmark values, $\mathcal{H}_I$, and m_ϕ are the least for GH-BM2. As a result of this, $T_{\rm rh}/\lambda_{12}$ is the max for this particular benchmark.

Now, using Γ_ϕ from Eq. (33) in Eq. (31), we get

$$\frac{T_{\rm max}}{T_{\rm rh}} \approx 1.67 \left(\frac{\mathcal{H}_I m_\phi}{\lambda_{12}^2}\right)^{1/4}. \quad (35)$$

Thus, for a specific benchmark value, $T_{\rm max}/T_{\rm rh}$ is highest for the lowest value of λ_{12}. The lower bound on λ_{12} can be obtained from the condition $T_{\rm rh} \gtrsim 4$ Mev (or, $\mathcal{O}(1$ MeV), depending on the theory) which is required for successful big bang nucleosynthesis (BBN) and this leads to $\lambda_{12}/M_P \gtrsim 5.5449 \times 10^{-23}$ (for GH-BM1), $\gtrsim 4.6885 \times 10^{-23}$ (for GH-BM2), and $\gtrsim 5.1603 \times 10^{-23}$ (for GH-BM3). For these lower limits of λ_{12}, the highest possible value of $T_{\rm max}/T_{\rm rh} \sim 4.9418 \times 10^8$ (for GH-BM1), $\sim 2.4586 \times 10^8$ (for GH-BM2), and $\sim 5.2695 \times 10^8$ (for GH-BM3). For higher values of λ_{12}, i.e., for larger values of $T_{\rm rh}$, $T_{\rm max}/T_{\rm rh}$ decreases as mentioned earlier, and it is displayed in Fig. 2. These values can also be approximated using Fig. 2 which shows how $T_{\rm max}/T_{\rm rh}$ declines as $T_{\rm rh}$ increases for two benchmark values—GH-BM2, and GH-BM3. Since $T_{\rm max}/T_{\rm rh}$ is almost the same for GH-BM1 and GH-BM3, GH-BM1 is not included in that figure. The gray-colored vertical stripe on the left of the figure indicates bound on the $T_{\rm rh}$ coming from the fact that $T_{\rm rh} \geq 4$ MeV [for successfully occurring of big bang nucleosynthesis (BBN)] [85]. The colored boxes on the lines represent the maximum permissible values of $T_{\rm rh}$ which correspond to the maximum allowable values of λ_{12} from Table III. The colored stripes on the right of the figure indicate that those values of $T_{\rm rh}$ are not allowed from the stability analysis.
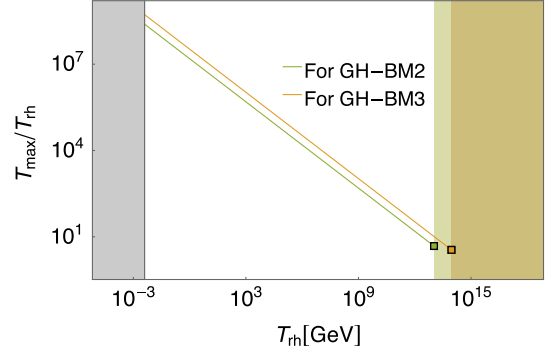

FIG. 2. This figure showcases the variation of $T_{\rm max}/T_{\rm rh}$ against $T_{\rm rh}$ for two benchmark values GH-BM2 and GH-BM3 from Table I. The square colored boxes on the lines represent the maximum permissible values of $T_{\rm rh}$ which correspond to the maximum allowable values of λ_{12} from Table III. The vertical stripe on the left of the plot, highlighted in gray, displays lower bound on $T_{\rm rh}$ i.e. $T_{\rm rh} \gtrsim 4$ MeV. The colorful stripes on the right side of the plot show that there are no permissible values of $T_{\rm rh}$ based on stability analysis of the corresponding benchmark values.

Next, we consider the production of DM during reheating. If n_χ is the number density of χ, then the conservation equation of the comoving number density, N_χ which is defined as $n_\chi a^3$, is

$$\frac{dN_\chi}{dt} = a^3 \gamma, \quad (36)$$

in which t is the physical time, and $\gamma \equiv \gamma(t)$ which is the rate of production of χ, has a quartic mass-dimension.

When the temperature of the universe is $T_{\rm max} > T > T_{\rm rh}$, then [58]

$$\mathcal{H} = \frac{\pi}{3} \sqrt{\frac{g_\star}{10}} \frac{T^4}{M_P T_{\rm rh}^2}. \quad (37)$$

During that period, the energy density of the universe is dominated by ρ_ϕ. Thus, from the first Friedman equation, we get

$$\rho_\phi = \frac{\pi^2 g_\star}{30} \frac{T^8}{T_{\rm rh}^4}. \quad (38)$$

If we combine Eq. (27) with Eq. (38), and then using Eq. (37) into Eq. (36), we obtain

$$\frac{dN_\chi}{dT} = -\frac{8M_P}{\pi} \left(\frac{10}{g_\star}\right)^{1/2} \frac{T_{\rm rh}^{10}}{T^{13}} a^3(T_{\rm rh}) \gamma. \quad (39)$$

To filter out the effect of the expansion of the universe on the time evolution of n_χ [91], we define DM yield, Y_χ, as $Y_\chi = n_\chi(T)/s(T)$, where $s(T) = (2\pi^2/45)g_{\star,s}T^3$ and $g_{\star,s}$

refers to the effective number of degrees of freedom contributing to the entropy of the relativistic fluid. We assume that entropy density per comoving volume remains conserved once the reheating era is over. The energy density of χ continues to decrease with time, contributing to the cold dark matter (CDM) density of the present universe. Present day CDM yield can be calculated as [92]

$$Y_{\text{CDM},0} = \frac{\Omega_{\text{CDM}}\rho_{\text{crit}}}{s_0 m_\chi} = \frac{4.3. \times 10^{-10}}{m_\chi}, \tag{40}$$

where m_χ is expressed in GeV and we have used scaling factor for Hubble expansion rate $h_{\text{CMB}} \approx 0.674$, cold dark matter density of the universe $\Omega_{\text{CDM}} = 0.12 h_{\text{CMB}}^{-2}$, present day entropy density $s_0 = 2891.2$ cm^{-3}, and critical density of the Universe $\rho_{\text{crit}} = 1.053 \times 10^{-5} h_{\text{CMB}}^2$ GeV cm^{-3} (as we choose $k_B = c = 1$ unit) from Ref. [77]. Now, we estimate the yield of χ produced through decay or via scattering, and then compare with $Y_{\text{CDM},0}$ to determine the extent to which the produced χ contributes to the total CDM density of the present universe.

1. Inflaton decay

If χ is produced exclusively via the decay of inflaton ($\phi \to \bar{\chi}\chi$), then

$$\gamma = 2\text{Br}\Gamma \frac{\rho_\phi}{m_\phi}. \tag{41}$$

When we substitute this in Eq. (39), along with the assumption that the DM yield remains unaltered after the end of reheating to present day, we obtain the expression for the DM yield from the decay of inflaton as,

$$Y_{\chi,0} = \frac{N_\chi(T_{\text{rh}})}{s(T_{\text{rh}})a^3(T_{\text{rh}})} \tag{42}$$

$$\simeq \frac{3}{\pi} \frac{g_\star}{g_{\star,s}} \sqrt{\frac{10}{g_\star}} \frac{M_P \Gamma}{m_\phi T_{\text{rh}}} \text{Br} = \frac{3}{\pi} \frac{g_\star}{g_{\star,s}} \sqrt{\frac{10}{g_\star}} \frac{M_P}{T_{\text{rh}}} \frac{(y_\chi)^2}{8\pi} \tag{43}$$

$$= 1.163 \times 10^{-2} M_P \frac{y_\chi^2}{T_{\text{rh}}}. \tag{44}$$

Here, we assume $g_{\star,s} = g_\star$. Equating Eq. (44) with Eq. (40), we get the condition to generate the complete CDM energy density in terms of the DM mass to be

$$T_{\text{rh}} \simeq 6.49 \times 10^{25} y_\chi^2 m_\chi. \tag{45}$$

Lines for different values of y_χ from Eq. (45) are shown as discontinuous inclined lines on (T_{rh}, m_χ) plane in log-log scale in Fig. 3. These lines actually correspond to χ being produced from the decay of inflaton and also producing the total CDM density of the present-day
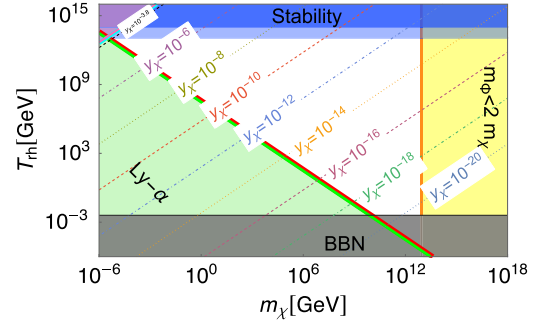

FIG. 3. The plot showcases the variation in the permissible region on (T_{rh}, m_χ) plane as well as allowed range of y_χ, specifically for benchmark values GH-BM1 and GH-BM2. The unshaded region on this plane represents the allowed region, and the dashed or dashed-dotted lines that intersect it correspond to Eq. (45) for different values of y_χ satisfying present-day CDM density. The regions shaded in light neon blue (horizontal stripe at the top of the figure) and yellow (vertical stripe on the right-hand side) represent the bounds from the permissible upper bound on λ_{12} (from stability analysis) and the maximum possible value of m_χ, while the purple, and green shaded area show the bounds on y_χ from stability analysis, and Ly-α bound on the mass of DM [58] [see also Eq. (47)] for GH-BM2. The same bounds for GH-BM1 are presented by deep neon blue-shaded region, and orange solid line, cyan and red colored solid lines. The gray shaded stripe at the bottom is for bound from BBN (i.e. T_{rh} should be $\gtrsim 4$ MeV). This figure shows that $y_\chi \sim 10^{-8}$ is allowed for GH-BM1, but not for GH-BM2.

universe. Figure 3 actually shows how the permissible region which is shown as white region on (T_{rh}, m_χ) plane, varies with benchmarks. Bounds on this plane are from: the largest permissible value of λ_{12} and y_χ from stability analysis of Table III (neon blue-colored stripe at the top of the plot and purple-colored wedge-shaped region at the left-top of the plot for GH-BM1, while deep neon blue-colored stripe at the top of the plot and cyan-colored wedge-shaped region at the left-top of the plot for GH-BM2), BBN temperature: $T_{\text{rh}} \gtrsim 4$ MeV (gray colored horizontal stripe at the bottom of the plot), and Ly-α bound from Eq. (47): $T_{\text{rh}} \gtrsim (2m_\phi)/m_\chi$ (region shaded with green color for GH-BM1 and red color (line) for GH-BM2) and the maximum possible value of $m_\chi = m_\phi/2$ (vertical stripe at the right, shaded with yellow color for GH-BM1 and orange color for GH-BM2). The allowed range of y_χ shown by inclined, discontinuous lines passing through the white unshaded region. While the allowed range of y_χ are nearly the same for both chosen benchmark values, the range of y_χ for CW-BM2 is narrower. For example, $y_\chi \sim 10^{-3.8}$ is not allowed for CW-BM2 but permissible for CW-BM1. The allowed range of m_χ for 3.1738×10^{-6} GeV $\lesssim m_\chi \lesssim 1.0297 \times 10^{13}$ GeV for GH-BM1 and 2.7836×10^{-6} GeV$\lesssim m_\chi \lesssim 7.3621 \times 10^{12}$ GeV for GH-BM2. If both y_χ and m_χ fall within these ranges, then it can satisfy two conditions simultaneously: (i) produced solely through the decay of

inflation, and (ii) produce the total CDM density of the universe. All the aforementioned bounds vary for three benchmark values mentioned in Table I. One of the two reason for this variation is different values of m_ϕ, which is already mentioned in Table IV, with m_ϕ for GH-BM1 > for GH-BM2. Additionally, the upper limit of the possible value of λ_{12}/M_P from stability analysis for GH-BM1 > GH-BM2. These factor imposes lower limit on m_χ as 2783.64 GeV for GH-BM2. However, on this $(T_{\rm rh}, m_\chi)$ plane more stringent bounds can be drawn from gravitino production. Nevertheless, we ignore this bound in our analysis as we do not take supersymmetry into account.

To derive the Ly-α bound used in Fig. 3 it is assumed that χ being feebly interacting BSM particle, its momentum only decreases due to red-shift and thus [58]

$$p_0 = \frac{a_{\rm rh}}{a_0} p_{\rm rh} \simeq 3 \times 10^{-14} \frac{m_\phi}{T_{\rm rh}} \, {\rm GeV}, \qquad (46)$$

where $p_{\rm rh}$ is the momentum of χ at the time of reheating (i.e., at temperature $T_{\rm rh}$) and $p_{\rm rh}$ is assumed as the initial momentum of the DM particles. Similarly, p_0, a_0, and $a_{\rm rh}$ are the momentum, cosmological scale factor today and at the time of reheating, respectively. The maximum possible value of $p_{\rm rh}$ is $p_{\rm rh} = m_\phi/2$. If we approximate $p_0 = m_\chi v_\chi$, where v_χ is the present day velocity of χ particles, then, using upper bound on $v_x/c \lesssim 1.8 \times 10^{-8}$ and $m_c \gtrsim 3.5$ keV (for further details about bound on the mass of warm dark matter from Ly-α see references within [59]) such that χ as a warm dark matter particle does not negatively impact on structure formation, we can obtain that

$$m_\chi \gtrsim 2 \frac{m_\phi}{T_{\rm rh}}, \qquad (47)$$

where m_χ is expressed in keV.

2. DM from scattering

In this subsection, we look at three important 2-to-2 scattering mechanisms for DM production: from scattering of nonrelativistic inflaton with graviton as the mediator, scattering of SM particles with graviton as mediator, and scattering of SM particles with inflaton as mediator. If $Y_{\rm IS,0}$, $Y_{{\rm SM}g,0}$, and $Y_{{\rm SM}i,0}$ are respectively the DM yield produced only via those three scattering channels, then [58]

$$Y_{\rm IS,0} \simeq \frac{g_\star^2}{81920 g_{\star,s}} \sqrt{\frac{10}{g_\star}} \left(\frac{T_{\rm rh}}{M_P}\right)^3 \left[\left(\frac{T_{\rm max}}{T_{\rm rh}}\right)^4 - 1\right] \frac{m_\chi^2}{m_\phi^2}$$
$$\times \left(1 - \frac{m_\chi^2}{m_\phi^2}\right)^{3/2}. \qquad (48)$$

$$Y_{{\rm SM}g,0} = \begin{cases} \frac{45 \alpha_{\rm DM}}{2\pi^3 g_{\star,s}} \sqrt{\frac{10}{g_\star}} \left(\frac{T_{\rm rh}}{M_P}\right)^3, & {\rm for} \ m_\chi \ll T_{\rm rh}, \\ \frac{45 \alpha_{\rm DM}}{2\pi^3 g_{\star,s}} \sqrt{\frac{10}{g_\star}} \frac{T_{\rm rh}^7}{M_P^3 m_\chi^4}, & {\rm for} \ T_{\rm max} \gg m_\chi \gg T_{\rm rh}. \end{cases} \qquad (49)$$

$$Y_{{\rm SM}i,0} \simeq \frac{135 y_\chi^2 \lambda_{12}^2}{4\pi^8 g_{\star,s}} \sqrt{\frac{10}{g_\star} \frac{M_P T_{\rm rh}}{m_\phi^4}}, \quad {\rm for} \ T_{\rm rh} \ll m_\phi, T_{\rm rh} > T. \quad (50)$$

In Eq. (49), $\alpha_{\rm DM} = 1.1 \times 10^{-3}$ [17] and it is related to the coupling of gravitational interaction. In Eq. (48), $Y_{\rm IS,0}$ is increasing function of $T_{\rm rh}$. Now, from the stability analysis of Table III, maximum permissible value for $T_{\rm rh}$ are

$$T_{\rm rh, allowable} = \begin{cases} 9.2027 \times 10^{13} \ {\rm GeV} & {\rm for \ GH\text{-}BM1}, \\ 1.059 \times 10^{13} \ {\rm GeV} & {\rm for \ GH\text{-}BM2}, \\ 9.0297 \times 10^{13} \ {\rm GeV} & {\rm for \ GH\text{-}BM3}. \end{cases} \quad (51)$$

For $T_{\rm rh} \sim T_{\rm rh, allowable}$, $T_{\rm max}/T_{\rm rh} \sim 3.2581$ for GH-BM1, ~ 4.7783 for GH-BM2, and ~ 3.5072 for GH-BM3. Now, if we choose $T_{\rm rh} \sim T_{\rm rh, allowable}$ from Eq. (51), then, in order to achieve $Y_{\rm IS,0} \sim Y_{\rm CDM,0}$, it is required that m_χ should be $m_\chi{}^{\rm IS,0}$ where

$$m_\chi{}^{\rm IS,0} \sim \begin{cases} 4.1722 \times 10^{10} \ {\rm GeV} & {\rm for \ GH\text{-}BM1}, \\ 1.7358 \times 10^{11} \ {\rm GeV} & {\rm for \ GH\text{-}BM2}, \\ 3.4993 \times 10^{10} \ {\rm GeV} & {\rm for \ GH\text{-}BM3}. \end{cases} \quad (52)$$

Thus, to achieve comparable values of $Y_{\rm IS,0}$ and $Y_{\rm CDM,0}$, we need $m_\chi > m_\chi{}^{\rm IS,0}$ for $T_{\rm rh} < T_{\rm rh, allowable}$. Hence, if χ is produced exclusively only through the 2-to-2 scattering of inflaton via graviton mediation and contributes completely to the total CDM relic density, the required condition is $m_\chi \gtrsim m_\chi{}^{\rm IS,0}$ for $T_{\rm rh} \lesssim T_{\rm rh, allowable}$.

For DM production solely through scattering of SM particles with graviton as mediator and for $(m_\chi \gg T_{\rm rh})$ and with $T_{\rm rh} \sim T_{\rm rh, allowable}$

$$Y_{{\rm SM}g,0} \sim \begin{cases} 1.2903 \times 10^{-19} & {\rm for \ GH\text{-}BM1}, \\ 1.9663 \times 10^{-22} & {\rm for \ GH\text{-}BM2}, \\ 1.2189 \times 10^{-19} & {\rm for \ GH\text{-}BM3}. \end{cases} \quad (53)$$

Consequently, in order to satisfy $Y_{\rm IS,0} \sim Y_{\rm CDM,0}$, and for $T_{\rm rh} \lesssim T_{\rm rh, allowable}$, it is required that

$$m_\chi \gtrsim \begin{cases} 3.3326 \times 10^9 \ {\rm GeV} & {\rm for \ GH\text{-}BM1}, \\ 2.1868 \times 10^{12} \ {\rm GeV} & {\rm for \ GH\text{-}BM2}, \\ 3.5279 \times 10^9 \ {\rm GeV} & {\rm for \ GH\text{-}BM3}. \end{cases} \quad (54)$$

Therefore, from Eq. (54) we can deduce that DM particles produced solely though this specific scattering channel (2-to-2 scattering of SM particles with graviton as mediator with $m_\chi \ll T_{\rm rh}$) can contribute to the total CDM density, provided that m_χ is very high. However, for $(T_{\rm max} \gg m_\chi \gg T_{\rm rh})$ and $Y_{{\rm SM}g,0} = Y_{\rm CDM,0}$, we get

$$\frac{T_{\rm rh}^{\rm SM g,0}}{\rm GeV} = 7.1389 \times 10^{12} f_{T_{\rm rh}}^{-3/4}, \quad (55)$$

where we have assumed $T_{\rm rh} = m_\chi f_{T_{\rm rh}}, f_{T_{\rm rh}}$ being a fractional number much less than 1. As the value of $f_{T_{\rm rh}}$ decreases, $T_{\rm rh}^{\rm SM g,0}$ increases. For $f_{T_{\rm rh}} \sim 0.6$, $T_{\rm rh}^{\rm SM g,0} \sim \mathcal{O}(10^{13})$. However, for $T_{\rm rh} \sim \mathcal{O}(10^{13})$, $T_{\rm max}/T_{\rm rh} \sim 3$ [see Eq. (51)]. Therefore, it seems less probable, that satisfying the condition $T_{\rm max} \gg m_\chi \gg T_{\rm rh}, \chi$ produced through this scattering process (2-to-2 scattering of SM particles with graviton as mediator with $T_{\rm max} \gg m_\chi \gg T_{\rm rh}$) contributes 100% of the total CDM density.

Now we consider production of χ via 2-to-2 scattering of SM particles with inflaton as mediator (along with the constraint $T_{\rm rh} \ll m_\phi$). The condition that $Y_{{\rm SM}i,0}$ [from Eq. (50)] contributes a fraction f_χ (f_χ is a dimensionless fractional number) of total CDM relic density, then we obtain (in GeV)

$$m_\chi^{{\rm SM}i,0} = 4.2164 \times 10^{-5} \frac{m_\phi^4}{T_{\rm rh}, M_P y_\chi^2 \lambda_{12}^2} f_\chi. \quad (56)$$

Therefore, as values of y_χ and λ_{12} decreases the value of $m_\chi^{{\rm SM}i,0}$ increases. Now, using $T_{\rm rh} = f_\phi m_\phi$ where f_ϕ is fractional ($\ll 1$) dimensionless number, in Eq. (28), we get (in GeV)

$$m_\chi^{{\rm SM}i,0} = 3.2689 \times 10^{-7} \frac{f_\chi}{y_\chi^2 f_\phi^3}. \quad (57)$$

For the maximum permissible values of y_χ (from Table III) $m_\chi^{{\rm SM}i,0}$ becomes

$$m_\chi^{{\rm SM}i,0} = \begin{cases} 5.2090 \frac{f_\chi}{f_\phi^3} {\rm GeV} & ({\rm for~GH\text{-}BM1}), \\ 4.4239 \frac{f_\chi}{f_\phi^3} {\rm GeV} & ({\rm for~GH\text{-}BM2}), \\ 2.3828 \frac{f_\chi}{f_\phi^3} {\rm GeV} & ({\rm for~GH\text{-}BM}). \end{cases} \quad (58)$$

If $f_\chi \sim 1$ and $f_\phi \sim 10^{-2}$, then for $m_\chi^{{\rm SM}i,0} \sim \mathcal{O}(10^8)$ GeV, χ produced through this scattering channel (2-to-2 scattering of SM particles with inflaton as mediator with $T_{\rm rh} \ll m_\phi$) can contribute total CDM relic density.

Therefore, if χ is produced solely via either of the three scattering processes we have considered (i.e., 2-to-2 scattering of nonrelativistic inflaton with graviton as the

mediator, 2-to-2 scattering of SM particles with graviton as mediator with $m_\chi \ll T_{\rm rh}$, and 2-to-2 scattering of SM particles with inflaton as mediator with $T_{\rm rh} \ll m_\phi$), for GH inflation, then produced χ can contribute up to 100% of the total CDM relic density of the present universe.

IV. COLEMAN-WEINBERG INFLATION

If we consider a SM gauge singlet BSM field as the inflaton with quartic potential, the presence of self-interaction or Yukawa interaction in the Lagrangian density can give rise to quantum corrections. When such quantum loop corrections originating from interaction terms, UV completions [93], etc., are included, the effective potential for inflaton is given by [64,94]

$$V_{\rm CW}(\phi) = \frac{A\mathcal{Q}^4}{4} + A\phi^4 \left[\log\left(\frac{\phi}{\mathcal{Q}}\right) - \frac{1}{4} \right], \quad (59)$$

where $\mathcal{Q}$ represents the renormalization scale, and the inclusion of the term $\frac{A\mathcal{Q}^4}{4}$ is to ensure that the value of the potential is $\gtrsim 0$, even at its minimum. This Coleman-Weinberg (CW) inflationary scenario involves inflation beginning near $\phi = 0$ and then the inflaton travels toward $\phi_{\rm min}$, the minimum of the potential of Eq. (59). The benchmark values of CW inflationary scenario are mentioned in Table V and the $n_s - r$ predictions for the two benchmark values from Table V are shown in Fig. 4. The predicted value r for benchmark CW-BM1 and CW-BM2 fall within 1-σ and 2-σ best-fit contour of *Planck*2018+ BICEP3 (2022)+*Keck Array*2018 data and SO analysis, respectively.

A. Stability analysis for CW inflation

Here, we follow steps similar to that followed in Sec. III A, to determine the maximum permissible value of λ_{12} and y_χ, considering $V_{\rm tree}(\phi) \equiv V_{\rm CW}(\phi)$. Subsequently, we get

$$V'_{\rm tree}(\phi) \equiv V'_{\rm CW}(\phi) = 4A\phi^3 \left(\log\left(\frac{\phi}{v}\right) - \frac{1}{4} \right) + A\phi^3, \quad (60)$$

$$V''_{\rm tree}(\phi) \equiv V''_{\rm CW}(\phi) = 12A\phi^2 \left(\log\left(\frac{\phi}{v}\right) - \frac{1}{4} \right) + 7A\phi^2. \quad (61)$$

The maximum allowable values for λ_{12} and y_χ are presented in Table VI. The results from the table lead us to the conclusion that the upper limits for these couplings are as follows: $y_\chi < 5.5257 \times 10^{-4}$, $< 5.8920 \times 10^{-4}$, and

TABLE V. Benchmark values for CW inflationary model (for $\mathcal{N}_{\rm CMB} \approx 60$).

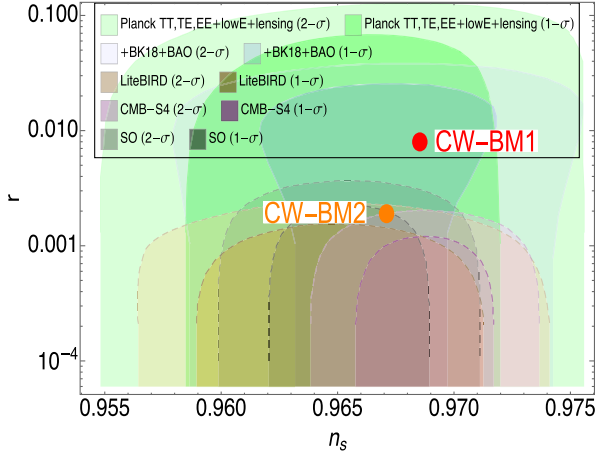| Benchmark	$\mathcal{Q}/M_P$	ϕ_*/M_P	$\phi_{\rm end}/M_P$	n_s	$r \times 10^3$	$A \times 10^{14}$
CW-BM1	16.4800	4.8450	8.4229	0.9685	7.9849	1.4075
CW-BM2	12.0500	2.3000	4.1520	0.9671	1.9091	1.1370

FIG. 4. The predicted values of n_s, r for the two benchmark values from Table V for CW slow roll inflationary scenario are displayed as colored circular dots. In addition, this figure also displays 2-σ and 1-$\sigma(n_s, r)$ best-fit contours from the *Planck* 2018+BICEP, as well as additional upcoming CMB observations mentioned earlier in Fig. 1.

$\lambda_{12}/M_P < 2.8864 \times 10^{-6}$, $< 1.4345 \times 10^{-6}$ for CW-BM1, and CW-BM2, respectively.

B. Reheating and production of DM from inflaton decay

In this section, we assume akin to what we have made for GH inflationary scenario in Sec. III B that following the end of slow roll inflationary phase, inflaton quickly descends to the minimum of the potential $V_{\mathrm{CW}}(\phi)$ and subsequently oscillates quasiperiodically about a quadratic minimum. The minimum of $V_{\mathrm{CW}}(\phi)$ is located at $\phi = \mathcal{Q}$, and $m_\phi, \Gamma_\phi, T_{\mathrm{rh}}$, and $\mathcal{H}_I$ for CW inflationary scenario are listed in Table VII. $\mathcal{H}_I$ for CW inflationary model is defined as

$$\mathcal{H}_I = \sqrt{\frac{V_{\mathrm{CW}}(\phi_{\mathrm{end}})}{3M_P^2}}. \tag{62}$$

From Table VII we see that the difference between the values of $\mathcal{H}_I/M_P$ is not very large for both benchmarks CW-BM1 and CW-BM2. The same is also true for the parameters $T_{\mathrm{rh}}/\lambda_{12}$ and m_ϕ/M_P for the two chosen benchmark values. Therefore, we present $T_{\max}/T_{\mathrm{rh}}$ [defined in Eq. (31)] against T_{rh} as solid line only for CW-BM1 in

Fig. 5. The gray-colored vertical stripe on the left of the figure shows a limit on T_{rh} due to the requirement that T_{rh} must be ≥ 4 MeV. On the right-hand side of the figure, there is a colored stripe that signifies that those T_{rh} values are not permitted based on the stability analysis from Table VI. The value of $T_{\max}/T_{\mathrm{rh}}$ is highest for $T_{\mathrm{rh}} \sim 4$ MeV and the ratio decreases as the value of T_{rh} increases. This pattern closely resembles the observed behavior illustrated in Fig. 2 for the GH inflationary scenario. The maximum value of $T_{\max}/T_{\mathrm{rh}}$ is $\sim 6.4796 \times 10^8$ for CW-BM1 (and the maximum value of $T_{\max}/T_{\mathrm{rh}} \sim 5.5401 \times 10^8$ for CW-BM2 at $T_{\mathrm{rh}} \sim 4$ MeV). Furthermore, lower bound on T_{rh} leads to establishing the minimum permissible value of λ_{12} which are $\lambda_{12}/M_P \gtrsim 3.7431 \times 10^{-23}$ for CW-BM1, and $\lambda_{12}/M_P \gtrsim 3.0344 \times 10^{-23}$ for CW-BM2.

Similarly, Fig. 6 shows $(T_{\mathrm{rh}}, m_\chi)$ plane for CW inflation, particularly for benchmark CW-BM1. The discontinuous lines correspond to Eq. (45). The bounds on this plane are similar to Fig. 3 the largest permissible value of λ_{12} and y_χ from stability analysis of Table VI (neon blue-colored horizontal stripe at the top of the plot and purple-colored wedge-shaped region at the left-top corner of the plot), BBN temperature: $T_{\mathrm{rh}} \gtrsim 4$ MeV (gray colored horizontal stripe at the bottom of the plot), and Ly-α bound from Eq. (47): $T_{\mathrm{rh}} \gtrsim (2m_\phi)/m_\chi$ (region shaded with green color) and maximum possible value of $m_\chi = m_\phi/2$ (vertical stripe at the right, shaded with yellow color). The unshaded region is allowed on $(T_{\mathrm{rh}}, m_\chi)$ plane and thus if $10^{-4} \gtrsim y_\chi \gtrsim 10^{-20}$ $(9.7318 \times 10^{-7}\,\mathrm{GeV} \lesssim m_\chi \lesssim 4.6924 \times 10^{12}\,\mathrm{GeV})$, then χ produced only via the decay of inflaton for the benchmark CW-BM1 in CW inflationary scenario can contribute up to 100% of the entire CDM relic density of the present universe. Since, m_ϕ and $\mathcal{H}_I$ are almost similar for CW-BM1 and CW-BM2 (see Table VII), Ly $-\alpha$ and $m_\chi \lesssim m_\phi/2$ are almost similar for both benchmarks. However, significant difference on the allowed region on $(T_{\mathrm{rh}}, m_\chi)$ for the two benchmark values comes the maximum permissible value of T_{rh} from stability analysis of Table VI. As a result, the permitted range of m_χ for CW-BM2 is almost similar $\sim 7.3988 \times 10^{-7}\,\mathrm{GeV} \lesssim m_\chi \lesssim 3.0837 \times 10^{12}$ GeV.

1. DM from scattering

Similar to GH inflationary scenario, there is an upper limit on λ_{12} from the stability analysis in this case

TABLE VI. Allowed upper limit of y_χ and λ_{12} for the benchmark values from Table V.

	Stability for y_χ		Stability for λ_{12}	
Benchmark	About $\mu = \phi_*$	About $\mu = \phi_{\mathrm{end}}$	About $\mu = \phi_*$	About $\mu = \phi_{\mathrm{end}}$
CW-BM1	$y_\chi < 6.4530 \times 10^{-4}$	$y_\chi < 5.5257 \times 10^{-4}$	$\lambda_{12}/M_P < 2.8864 \times 10^{-6}$	$\lambda_{12}/M_P < 3.6784 \times 10^{-6}$
CW-BM2	$y_\chi < 6.3004 \times 10^{-4}$	$y_\chi < 5.8920 \times 10^{-4}$	$\lambda_{12}/M_P < 1.4345 \times 10^{-6}$	$\lambda_{12}/M_P < 2.0618 \times 10^{-6}$

TABLE VII. $m_\phi, \Gamma_\phi, T_{\rm rh}$, and $\mathcal{H}_I$ for the benchmark values from Table V.

Benchmark	m_ϕ/M_P (Sec. III B)	$\Gamma_\phi M_P$ [Eq. (33)]	$T_{\rm rh}/\lambda_{12}$ [Eq. (28)]	$\mathcal{H}_I/M_P$ [Eq. (62)]
CW-BM1	3.9103×10^{-6}	$10175.3\lambda_{12}^2$	44.5268	8.0473×10^{-6}
CW-BM2	2.5698×10^{-6}	$15483.5\lambda_{12}^2$	54.9265	4.3006×10^{-6}

(CW inflation). Therefore, upper limit on $T_{\rm rh}$ from stability analysis

$$T_{\rm rh, allowable} = \begin{cases} 3.0845 \times 10^{14} & \text{for CW-BM1,} \\ 1.8911 \times 10^{14} & \text{for CW-BM2.} \end{cases} \quad (63)$$

And for such maximum possible values of $T_{\rm rh}$, $T_{\max}/T_{\rm rh, allowable} > 1$ is maintained. Now, for $T_{\rm rh} \sim T_{\rm rh, allowable}$, and the condition $Y_{\rm IS,0} \sim Y_{\rm CDM,0}$ [from Eqs. (45) and (48)], the value of m_χ is

$$m_\chi^{\rm IS,0} \sim \begin{cases} 1.1602 \times 10^{10} \text{ GeV} & \text{for CW-BM1,} \\ 1.2677 \times 10^{10} \text{ GeV} & \text{for CW-BM2.} \end{cases} \quad (64)$$

Therefore, for CW, the required condition to make $Y_{\rm IS,0} \sim Y_{\rm CDM,0}$ is $m_\chi \gtrsim m_\chi^{\rm IS,0}$ for $T_{\rm rh} \lesssim T_{\rm rh, allowable}$.

In the scenario where DM particles are produced through the scattering process involving SM particles and the mediator being a graviton (with $m_\chi \ll T_{\rm rh}$) [Eq. (49)], assuming $T_{\rm rh} \sim T_{\rm rh, allowable}$, we obtain

$$Y_{\rm SMg,0} = \begin{cases} 4.8586 \times 10^{-18} & \text{(for CW-BM1),} \\ 1.1196 \times 10^{-18} & \text{(for CW-BM2).} \end{cases} \quad (65)$$
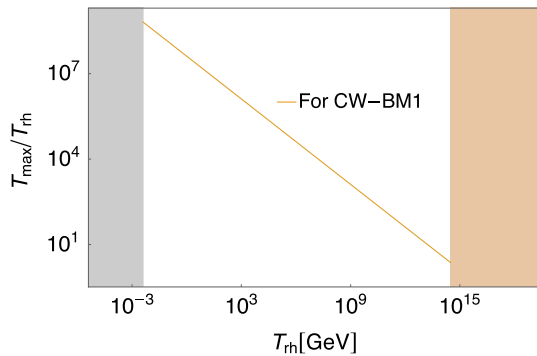

FIG. 5. This figure showcases the variation of $T_{\max}/T_{\rm rh}$ against $T_{\rm rh}$ for benchmark value CW-BM1 from Table V. The vertical stripe on the left of the plot, highlighted in gray, displays the lower bound on $T_{\rm rh}$, i.e., $T_{\rm rh} \gtrsim 4$ MeV. The colorful stripe on the right of the plot shows that there is no permissible value of $T_{\rm rh}$ based on stability analysis of the corresponding benchmark value from Table VI.
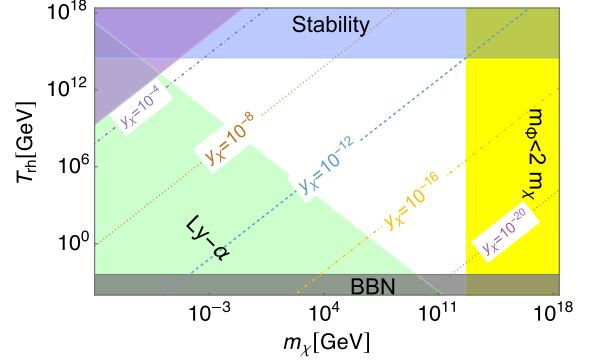

FIG. 6. The region without any color on $(T_{\rm rh}, m_\chi)$ plane, depicted on log-log scale, indicates the allowed region for the benchmark value CW-BM1 from Table V. The dashed or dashed-dotted lines that intersect the white region correspond to Eq. (45) for various values of y_χ that satisfy present-day CDM relic density. The colored regions on this plane represent various bounds—stability analysis: the maximum allowed value of $T_{\rm rh}$ from the upper limit of λ_{12} from Table VI (neo blue colored horizontal stripe at the top) and the maximum allowed value of y_χ from Table VI (purple-colored wedge-shaped region at the top-left), from Ly-α bound on the mass of DM Eq. (47): green-colored region, and $m_\chi \lesssim m_\phi/2$: yellow colored vertical stripe on the right. The gray colored stripe at the bottom depicts that $T_{\rm rh}$ should be $\gtrsim 4$ MeV.

And thus to make $Y_{\rm SMg,0} \sim Y_{\rm CDM,0}$ [from Eq. (40)], we get

$$m_\chi \sim \begin{cases} 8.8503 \times 10^7 \text{ GeV} & \text{(for CW-BM1),} \\ 3.8407 \times 10^8 \text{ GeV} & \text{(for CW-BM2).} \end{cases} \quad (66)$$

Thus, to satisfy the CDM yield, m_χ should be greater than or equal to the values mentioned in Eq. (66).

However, it appears that the conclusion for CW is similar to GH inflation for 2-to-2 scattering of SM particles with graviton as mediator with $T_{\max} \gg m_\chi \gg T_{\rm rh}$ following Eq. (55). This is because $T_{\max}/T_{\rm rh} \sim 40$ for $T_{\rm rh} \sim 10^{12}$ GeV and $T_{\max}/T_{\rm rh, allowable} \sim 2$ for both CW-BM1 and CW-BM2 [see Eq. (63)].

For the production of χ via 2-to-2 scattering of SM particles with inflaton as mediator (along with the constraint $T_{\rm rh} \ll m_\phi$), the condition that $Y_{\rm SMi,0}$ contributes f_χ fraction of total CDM relic density [Eq. (57)] along with the maximum permissible values of y_χ (from Table VI)

$$m_\chi^{\rm SMi,0} = \begin{cases} 1.0706 \dfrac{f_\chi}{f_\phi^3} \text{ GeV} & \text{(for CW-BM1),} \\ 0.9416 \dfrac{f_\chi}{f_\phi^3} \text{ GeV} & \text{(for CW-BM2).} \end{cases} \quad (67)$$

Therefore, just like in GH inflationary scenario, if $f_\chi/f_\phi^3 \sim 1$, then $m_\chi \sim \mathcal{O}(1)$ GeV, while for $f_\chi/f_\phi^3 \sim 10^8$, $m_\chi \sim \mathcal{O}(10^7$–$10^8)$ GeV is required.

V. DISCUSSION AND CONCLUSION

In this study, we considered two distinct slow roll single-field inflationary scenarios: GH and CW with inflaton minimally coupled to gravity and suggested production of a nonthermal vectorlike fermionic particle χ during reheating era. For each inflationary model, we considered a set of benchmark values and for those set of benchmark values, we explored the permissible parameter space encompassing y_χ, m_χ, assuming that χ is a potential candidate for the CDM of the present universe. Salient features of our findings are as follows:

(i) For our chosen benchmarks, we found that r can be as small as 2.69×10^{-6} for small-field GH inflationary scenario (see Table I), and this predicted value fits inside 1-σ contour on (n_s, r) plane of *Planck*2018+BICEP3+*Keck Array*2018 as well as upcoming SO experiment. On the other hand, the lowest value of r we found for CW inflation is $\sim 1.9091 \times 10^{-3}$, which can be corroborated by upcoming SO (see Table V).

(ii) Using stability analysis and bound from BBN temperature, we computed the permissible upper limit for the coupling y_χ and permissible range for λ_{12} [defined in Eq. (4)] for GH and CW inflation and found $y_\chi < \mathcal{O}(10^{-4})$ and $\mathcal{O}(10^{-5}) \lesssim \lambda_{12} \lesssim \mathcal{O}(10^{12})$ (in GeV)(see Tables III and VI), and these limits varies with various benchmarks as well as inflationary models. The highest permissible value for y_χ is found for CW-BM2 and largest allowed range of λ_{12} for the CW-BM1 among all chosen benchmarks in both inflationary scenarios.

(iii) From Tables IV and VII, we infer that the value of m_ϕ is subject to alteration depending on benchmarks (and thus with inflationary parameters, including r) and inflationary scenarios, being highest ($\sim 2.0595 \times 10^{13}$ GeV) for GH-BM1 and lowest for CW-BM2 ($\sim 6.1675 \times 10^{12}$ GeV), consequently affecting $T_{\rm rh}$, Ly-α bound and maximum possible value of m_χ.

(iv) Figures 2 and 5 illustrates the variation of $T_{\rm max}/T_{\rm rh}$ against $T_{\rm rh}$ with the highest value of $T_{\rm max}/T_{\rm rh} \sim \mathcal{O}(10^8)$ at $T_{\rm rh} \sim 4$ MeV. However, $T_{\rm max}/T_{\rm rh}$ changes based on chosen benchmarks and thus depends on inflationary parameters, e.g., n_s, r, etc.

(v) Ensuring that χ is produced only through inflaton decay and contributes 100% of the total relic density of CDM of the present universe, Figs. 3 and 6 demonstrates that the allowed range of y_χ is $10^{-4} \gtrsim y_\chi \gtrsim 10^{-20}$ for both GH and CW inflationary scenarios. However, the allowed space on the $(T_{\rm rh}, m_\chi)$ plane, which determines the allowed range of y_χ, varies with benchmark values (for example, see Fig. 3) and thus depends on inflationary parameters.

(vi) Assuming that χ is produced via 2-to-2 scattering channels involving SM particles with $m_\chi \ll T_{\rm rh}$ or nonrelativistic inflaton (both processes are mediated by graviton) or through 2-to-2 scattering of SM particles with inflaton as mediator with $T_{\rm rh} \ll m_\phi$, it was found that the individual contributions from these scattering channels for each inflationary scenario can account for 100% of the total CDM yield of the present universe if $m_\chi \gtrsim \mathcal{O}(10^{10})$ GeV [see Eqs. (52) and (64)] and $m_\chi \gtrsim \mathcal{O}(10^9)$ GeV [see Eqs. (54) and (66)] and $m_\chi \gtrsim \mathcal{O}(10^8)$ GeV [for $T_{\rm rh} \sim 10^{-2} m_\phi$, see Eqs. (58) and (67)], respectively. However, depending on the inflationary parameters along with the specific model of inflation being considered, the precise range of m_χ undergoes variation. Nonetheless, the scattering channel involving SM particles mediated by graviton, where $T_{\rm max} \gg m_\chi \gg T_{\rm rh}$, appears to be less efficient in generating the overall relic density of CDM.

In this article, we considered generalized version of Hilltop inflation and Coleman-Weinberg inflationary scenario with nonminimal coupling to curvature scalar. Our study was focused on the reheating era which is preceded by slow roll inflation happening near the maximum of the potential. Along with the inflaton, we incorporated a fermionic SM singlet field into our analysis, which is expected to contribute to the CDM density of the present universe. The verification of such a model could possibly be achieved through the detection BB mode by future CMB experiments, e.g., CMB-S4, SO, and so on [75,95–104]. Presence of interaction with inflaton and DM particles may leave imprint on non-Gaussianities on CMB power spectrum and this can provide an alternative path to test our theory. However, exploring these aspects extends beyond the scope of this work.

[1] B. Carr and F. Kuhnel, Annu. Rev. Nucl. Part. Sci. **70**, 355 (2020).

[2] A. D. Dolgov and S. Porey, Bulg. Astron. J. **34**, 2021 (2019).

[3] J. McDonald, Phys. Rev. Lett. **88**, 091304 (2002).

[4] K.-Y. Choi and L. Roszkowski, AIP Conf. Proc. **805**, 30 (2005).

[5] A. Kusenko, Phys. Rev. Lett. **97**, 241301 (2006).

[6] K. Petraki and A. Kusenko, Phys. Rev. D **77**, 065014 (2008).

[7] L. J. Hall, K. Jedamzik, J. March-Russell, and S. M. West, J. High Energy Phys. 03 (2010) 080.

[8] N. Bernal, M. Heikinheimo, T. Tenkanen, K. Tuominen, and V. Vaskonen, Int. J. Mod. Phys. A **32**, 1730023 (2017).

[9] M. R. Haque and D. Maity, Phys. Rev. D **106**, 023506 (2022).

[10] M. R. Haque and D. Maity, Phys. Rev. D **107**, 043531 (2023).

[11] M. R. Haque, D. Maity, and R. Mondal, J. High Energy Phys. 09 (2023) 012.

[12] H. Baer, K.-Y. Choi, J. E. Kim, and L. Roszkowski, Phys. Rep. **555**, 1 (2015).

[13] M. Garny, M. Sandora, and M. S. Sloth, Phys. Rev. Lett. **116**, 101302 (2016).

[14] Y. Tang and Y.-L. Wu, Phys. Lett. B **758**, 402 (2016).

[15] Y. Tang and Y.-L. Wu, Phys. Lett. B **774**, 676 (2017).

[16] M. Garny, A. Palessandro, M. Sandora, and M. S. Sloth, J. Cosmol. Astropart. Phys. 02 (2018) 027.

[17] N. Bernal, M. Dutra, Y. Mambrini, K. Olive, M. Peloso, and M. Pierre, Phys. Rev. D **97**, 115020 (2018).

[18] A. Paul, A. Ghoshal, A. Chatterjee, and S. Pal, Eur. Phys. J. C **79**, 818 (2019).

[19] A. Ghoshal, Z. Lalak, and S. Porey, Phys. Rev. D **108**, 063030 (2023).

[20] A. A. Starobinsky, Phys. Lett. **91B**, 99 (1980).

[21] A. H. Guth, Phys. Rev. D **23**, 347 (1981).

[22] A. D. Linde, Phys. Lett. **108B**, 389 (1982).

[23] A. Albrecht and P. J. Steinhardt, Phys. Rev. Lett. **48**, 1220 (1982).

[24] R. N. Lerner and J. McDonald, Phys. Rev. D **80**, 123507 (2009).

[25] F. Kahlhoefer and J. McDonald, J. Cosmol. Astropart. Phys. 11 (2015) 015.

[26] T. E. Clark, B. Liu, S. T. Love, and T. ter Veldhuis, Phys. Rev. D **80**, 075019 (2009).

[27] V. V. Khoze, J. High Energy Phys. 11 (2013) 215.

[28] J. P. B. Almeida, N. Bernal, J. Rubio, and T. Tenkanen, J. Cosmol. Astropart. Phys. 03 (2019) 012.

[29] N. Bernal, A. Chatterjee, and A. Paul, J. Cosmol. Astropart. Phys. 12 (2018) 020.

[30] A. Aravind, M. Xiao, and J.-H. Yu, Phys. Rev. D **93**, 123513 (2016); **96**, 069901(E) (2017).

[31] G. Ballesteros, J. Redondo, A. Ringwald, and C. Tamarit, J. Cosmol. Astropart. Phys. 08 (2017) 001.

[32] D. Borah, P. S. B. Dev, and A. Kumar, Phys. Rev. D **99**, 055012 (2019).

[33] Y. Hamada, H. Kawai, and K.-y. Oda, J. High Energy Phys. 07 (2014) 026.

[34] S. Choubey and A. Kumar, J. High Energy Phys. 11 (2017) 080.

[35] J. M. Cline, M. Puel, and T. Toma, J. High Energy Phys. 05 (2020) 039.

[36] T. Tenkanen, J. High Energy Phys. 09 (2016) 049.

[37] Y. Abe, T. Toma, and K. Yoshioka, J. High Energy Phys. 03 (2021) 130.

[38] N. Okada, D. Raut, and Q. Shafi, Eur. Phys. J. C **80**, 1056 (2020).

[39] A. Das, S. Gola, S. Mandal, and N. Sinha, Phys. Lett. B **829**, 137117 (2022).

[40] A. Das, S. Oda, N. Okada, and D.-s. Takahashi, Phys. Rev. D **93**, 115038 (2016).

[41] A. Das, N. Okada, and N. Papapietro, Eur. Phys. J. C **77**, 122 (2017).

[42] R. Daido, F. Takahashi, and W. Yin, J. Cosmol. Astropart. Phys. 05 (2017) 044.

[43] M. Shaposhnikov and I. Tkachev, Phys. Lett. B **639**, 414 (2006).

[44] H. Davoudiasl, R. Kitano, T. Li, and H. Murayama, Phys. Lett. B **609**, 117 (2005).

[45] D. Hooper, G. Krnjaic, A. J. Long, and S. D. Mcdermott, Phys. Rev. Lett. **122**, 091802 (2019).

[46] Y. Ema, K. Hamaguchi, T. Moroi, and K. Nakayama, J. High Energy Phys. 01 (2017) 096.

[47] B. Barman, A. Ghoshal, B. Grzadkowski, and A. Socha, J. High Energy Phys. 07 (2023) 231.

[48] B. Barman, P. S. Bhupal Dev, and A. Ghoshal, Phys. Rev. D **108**, 035037 (2023).

[49] B. Barman and A. Ghoshal, J. Cosmol. Astropart. Phys. 10 (2022) 082.

[50] B. Barman, P. Ghosh, A. Ghoshal, and L. Mukherjee, J. Cosmol. Astropart. Phys. 08 (2022) 049.

[51] B. Barman and A. Ghoshal, J. Cosmol. Astropart. Phys. 03 (2022) 003.

[52] D. K. Ghosh, A. Ghoshal, and S. Jeesun, J. High Energy Phys. 01 (2024) 026.

[53] A. Chakraborty, M. R. Haque, D. Maity, and R. Mondal, Phys. Rev. D **108**, 023515 (2023).

[54] A. Ghoshal, L. Heurtier, and A. Paul, J. High Energy Phys. 12 (2022) 105.

[55] M. Berbig and A. Ghoshal, J. High Energy Phys. 05 (2023) 172.

[56] A. Ghoshal and P. Saha, Phys. Rev. D **109**, 023526 (2024).

[57] A. Ghoshal, M. Y. Khlopov, Z. Lalak, and S. Porey, arXiv:2306.08675.

[58] N. Bernal and Y. Xu, Eur. Phys. J. C **81**, 877 (2021).

[59] A. Ghoshal, G. Lambiase, S. Pal, A. Paul, and S. Porey, J. High Energy Phys. 09 (2022) 231.

[60] A. Ghoshal, G. Lambiase, S. Pal, A. Paul, and S. Porey, Symmetry **15**, 543 (2023).

[61] A. Ghoshal, G. Lambiase, S. Pal, A. Paul, and S. Porey, in *25th Workshop on What Comes Beyond the Standard Models?* (2022); arXiv:2211.15061.

[62] A. Ghoshal, Z. Lalak, S. Pal, and S. Porey, arXiv:2401.17262.

[63] Y. Akrami *et al.* (Planck Collaboration), Astron. Astrophys. **641**, A10 (2020).

[64] R. Kallosh and A. Linde, J. Cosmol. Astropart. Phys. 09 (2019) 030.

[65] R. Kallosh and A. Linde, Phys. Rev. D **100**, 123523 (2019).

[66] R. Kallosh and A. Linde, J. Cosmol. Astropart. Phys. 12 (2021) 008.

[67] H. G. Lillepalu and A. Racioppi, Eur. Phys. J. Plus **138,** 894 (2023).

[68] J. Hoffmann and D. Sloan, Phys. Rev. D **104,** 123542 (2021).

[69] L. Boubekeur and D. H. Lyth, J. Cosmol. Astropart. Phys. 07 (2005) 010.

[70] G. German, J. Cosmol. Astropart. Phys. 02 (2021) 034.

[71] K. Dimopoulos, Phys. Lett. B **809,** 135688 (2020).

[72] D. Baumann, *Cosmology* (Cambridge University Press, Cambridge, England, 2022).

[73] M. Hazumi *et al.* (LiteBIRD Collaboration), Proc. SPIE Int. Soc. Opt. Eng. **11443,** 114432F (2020).

[74] K. N. Abazajian *et al.* (CMB-S4 Collaboration), arXiv: 1610.02743.

[75] P. Ade *et al.* (Simons Observatory Collaboration), J. Cosmol. Astropart. Phys. 02 (2019) 056.

[76] N. Aghanim *et al.* (Planck Collaboration), Astron. Astrophys. **641,** A6 (2020); **652,** C4(E) (2021).

[77] R. L. Workman *et al.* (Particle Data Group Collaboration), Prog. Theor. Exp. Phys. **2022,** 083C01 (2022).

[78] P. A. R. Ade *et al.* (BICEP/Keck Collaboration), in *56th Rencontres de Moriond on Cosmology* (2022); arXiv:2203 .16556.

[79] P. A. R. Ade *et al.* (BICEP, Keck Collaborations), Phys. Rev. Lett. **127,** 151301 (2021).

[80] P. Campeti and E. Komatsu, Astrophys. J. **941,** 110 (2022).

[81] M. Drees and Y. Xu, J. Cosmol. Astropart. Phys. 09 (2021) 012.

[82] S. R. Coleman and E. J. Weinberg, Phys. Rev. D **7,** 1888 (1973).

[83] K. Enqvist, in *2010 European School of High Energy Physics* (2012); arXiv:1201.6164.

[84] M. A. G. Garcia, K. Kaneta, Y. Mambrini, and K. A. Olive, Phys. Rev. D **101,** 123507 (2020).

[85] G. F. Giudice, E. W. Kolb, and A. Riotto, Phys. Rev. D **64,** 023508 (2001).

[86] D. J. H. Chung, E. W. Kolb, and A. Riotto, Phys. Rev. D **60,** 063504 (1999).

[87] Y. Mambrini and K. A. Olive, Phys. Rev. D **103,** 115009 (2021).

[88] B. Barman, N. Bernal, Y. Xu, and O. Zapata, J. Cosmol. Astropart. Phys. 07 (2022) 019.

[89] K. D. Lozanov, arXiv:1907.04402.

[90] E. W. Kolb, A. Notari, and A. Riotto, Phys. Rev. D **68,** 123505 (2003).

[91] M. Lisanti, in *Theoretical Advanced Study Institute in Elementary Particle Physics: New Frontiers in Fields and Strings* (2017), pp. 399–446; arXiv:1603.03797.

[92] K. Garrett and G. Duda, Adv. Astron. **2011,** 968283 (2011).

[93] A. Racioppi, Phys. Rev. D **97,** 123514 (2018).

[94] G. Barenboim, E. J. Chun, and H. M. Lee, Phys. Lett. B **730,** 81 (2014).

[95] K. Abazajian *et al.* (CMB-S4 Collaboration), Astrophys. J. **926,** 54 (2022).

[96] M. Hazumi *et al.*, J. Low Temp. Phys. **194,** 443 (2019).

[97] D. Adak, A. Sen, S. Basak, J. Delabrouille, T. Ghosh, A. Rotti, G. Martínez-Solaeche, and T. Souradeep, Mon. Not. R. Astron. Soc. **514,** 3002 (2022).

[98] J. T. Sayre *et al.* (SPT Collaboration), Phys. Rev. D **101,** 122003 (2020).

[99] A. Suzuki *et al.* (POLARBEAR Collaboration), J. Low Temp. Phys. **184,** 805 (2016).

[100] S. Aiola *et al.* (ACT Collaboration), J. Cosmol. Astropart. Phys. 12 (2020) 047.

[101] K. Harrington *et al.*, Proc. SPIE Int. Soc. Opt. Eng. **9914,** 99141K (2016).

[102] G. Addamo *et al.* (LSPE Collaboration), J. Cosmol. Astropart. Phys. 08 (2021) 008.

[103] A. Mennella *et al.*, Universe **5,** 42 (2019).

[104] P. A. R. Ade *et al.* (SPIDER Collaboration), Astrophys. J. **927,** 174 (2022).